Adaptive Robust Controller Design For Dual-Stage Hard Disk Drives

H. D. Taghirad[†] and **P. Sheykholeslami**

Advanced **R**obotics and **A**utomated **S**ystems (**ARAS**)
Department of Electrical Engineering
K.N. Toosi University of Technology
[†]Taghirad@kntu.ac.ir

***Abstract* – In this paper, adaptive robust controllers are proposed for dual-stage hard disk drives. An Improved Desired Compensation ARC (IDCARC) scheme is proposed in this paper for both actuators of the system, in which the traditional ARC is powered by a dynamic adaptive term. Moreover, a simulation study of these controllers are presented, in which the controllers designed based on simple models for the subsystem are implemented on a more comprehensive, experimentally verified models of the system. Simulation result verifies the effectiveness of the IDCARC method in providing the required tracking, in presence of unstructured uncertainty for the models.**

Index Terms* - *Adaptive robust control, dual-stage hard disk drive, dynamic adaptation, robustness verification.

I. INTRODUCTION

The demand for continually increasing storage density, and reducing the data access time in commercial hard disk drives, necessitates the performance improvement of the head positioning systems. The servo system must achieve precise track following, the positioning of the head on a desired track, and fast track seeking, the transition from one track to another target track. The seeking time, should be minimized for faster data transmission rates. To meet these requirements the servo bandwidth of the head positioning system must be increased to lower the sensitivity to disturbances such as disk flutter vibrations, spindle motor run-out and external vibrations [1]. However, the servo bandwidth is mainly limited by the mechanical resonance of the head positioning system. The dual-stage actuation system offers one way to enlarge the servo bandwidth. Using high bandwidth secondary actuators mounted on the voice coil motor (VCM) has been investigated for many years [2], and is regarded as a feasible alternative to single stage servo systems. In this paper, a dual-stage hard disk drive system is considered, in which a push-pull type piezo-electric transducer (PZT) is used as a second-stage actuator, in addition to the first-stage VCM. The VCM has a large operating range and a low resonance frequency, and is used for coarse positioning. The PZT actuator has a small operating range and a high resonance frequency, and is used for fine positioning.

There are several attempts to develop unifying control algorithms, which work for both track seeking and track following [3-10]. Such control algorithms utilize LQR/LQG controller structure [4 , 5], composite nonlinear feedback control [6], gradient based track following [7], or other robust approaches for control [8]. Adaptive robust controller are also developed for single-stage hard disk servo systems [9], and by introducing dynamic adaptation into the adaptive structure of such controllers promising results in terms of fast and accurate tracking performance in presence of modeling uncertainty is obtained [10]. In this paper, this approach called IDCARC is implemented for the dual-stage disk drive servo system, and its closed loop performance is compared to that of ARC in presence of modeling uncertainty. To verify the robustness of such algorithms, experimentally verified models for the system [11], is used in the simulations. The simulation results applied on this model is promising to work well in practice.

The paper is organized as following, in section 2. the dynamic models for dual stage hard disk drives are described in detail, and high order linear models for HDD subsystems are given in addition to the modeling uncertainty. Section 3 is dedicated to the development of ARC and IDCARC methods and its theoretical performance characteristics. In section 3 the details of simulation studies, and the obtained results is elaborated.

II. DYNAMICS MODELS OF DUAL-STAGE HDD

Fig. 1 illustrates a schematic of a hard disk drive (HDD) with a dual-stage actuation system. Several disks are stacked on the spindle motor shaft, and each disk is accompanied by a pair of recording heads. Each head is attached to the tip of a suspension. The PZT actuator is placed between the suspension and the base plate. The VCM actuator moves the carriage, base plates, PZT actuators, suspensions and heads all together, and the PZT actuator drives only the suspension and the head. Therefore, the total movement of the head is composed of the individual movement provided to head by the VCM and PZT actuators. In order to control the position tip of the head of HDD with the stringent accuracy requirement, two controllers must be designed for the system, in which the

VCM closed loop feedback provides the course positioning, and the PZT actuator eliminates high frequency disturbances applied to the system. In order to model the individual actuators of the HDD let us start with a comprehensive nonlinear model for each actuator. A nonlinear model for the VCM is given as following [10]:

$$\begin{cases} \dot{x}_1 = x_2 \\ J\dot{x}_2 = u - Bx_2 - A_f Sign(\dot{y}) - F_{hys} + F_{hi} + F_d \end{cases} \quad (1)$$

$$y = x_1$$

in which, $x = [x_1, x_2]^T$ represent the state vector of the angular position and velocity, y is the position, J is the moment of inertia, u is the control input, B and A_f are coefficient of viscous and coulomb friction, respectively, F_{hys} and F_{hi} represent the effect of hysteresis loop and high frequencies uncertainties, respectively, and, F_d is the external disturbance. Similar nonlinear models can be derived for the PZT actuators in HDD's. In order to apply linear robust controllers to this problem, the nonlinear model of each actuator of the system is represented by a linear model and multiplicative uncertainty, using a systematic linear identification scheme. In this representation, the nominal model replicates the dynamic behavior of the system, only at nominal conditions, and all nonlinear interactions, unmodeled dynamics and the disturbances are encapsulated via an unstructured uncertainty representation. This idea is used extensively in many applications, where linear H_∞ or μ-synthesis schemes are used in controller design of some nonlinear systems [11,12].

In order to represent a system into this form, suppose the true system belongs to a family of plants $\prod$, which is defined by using the following perturbation to the nominal plant P_o:

$$\forall P(s) \in \Pi \qquad P(s) = \left(1 + \Delta(s) W(s)\right) P_o(s)$$

In this equation W(s) is a stable transfer function indicating the upper bound of uncertainty and Δ(s) indicates the admissible uncertainty block, which is a stable but unknown transfer function with $\|\Delta\|_\infty < 1$. In this general representation Δ(s)W(s) describes the normalized perturbation of the true plant from nominal plant, and is quantitatively determined through identification at each frequency:

$$\frac{P(j\omega)}{P_0(j\omega)} - 1 = \Delta(j\omega) W(j\omega)$$

In which $\|\Delta\|_\infty < 1$; hence,

$$\left| \frac{P(j\omega)}{P_0(j\omega)} - 1 \right| \le \left| W(j\omega) \right| , \ \forall \omega \quad (2)$$

Where, $|W(j\omega)|$ represents the amplitude of the uncertainty profile with respect to frequency. Nominal plant P_o, can be evaluated experimentally, through a series of frequency response estimates of the system in the operating regime. Linear identification for the system can be applied with different input amplitudes, while their outputs are measured and logged. By minimizing the least squares of the prediction error, from the set of input-output information, a set of linear

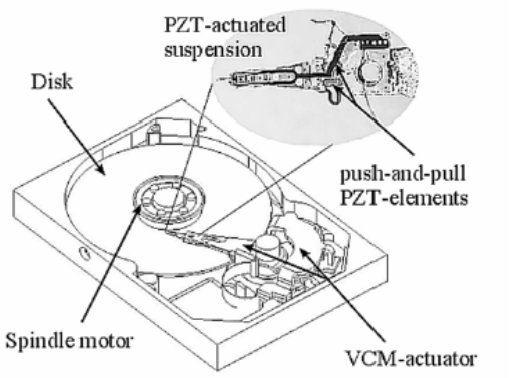

Fig. 1. Schematic of HDD with PZT actuator

models are estimated for the system, which can be considered as the set Π. The uncertainty upper bound $W(s)$, is then obtained using Equation (3), while the nominal plant P_o is selected from the average fit over all the individual identified plants. By this means, not only the nominal plant of the system is obtained, but also a measure of its perturbations, will be encapsulated by the multiplicative uncertainty.

Using this technique the actuator linear models are derived from experimental frequency response estimates of system [11]. In order to measure the tip position of the PZT actuator a Laser-Doppler-Scanning Vibrometer (LDV) is used in this reference. For each actuator, 21 frequency response estimates are then derived experimentally using a Dynamic Signal Analyzer (DSA), which are presented in Figs. 3 and 4. The nominal model of the actuators is derived by averaging all the frequency response estimates [11]. The nominal model of the VCM-actuator which is shown in Fig. 3, is a stable 12 order non-min phase system, whose pole zero patterns are given in Table I. The PZT actuator model is also a stable but 10 order non-min phase system whose zero-poles pattern are given in Table II.

The uncertainty profiles of the models are experimentally

TABLE I
POLES ZEROS PATTERN OF VCM NOMINAL MODEL

	Poles	Zeros
1,2	(-0.0230 ± 0.0896 j) ×10^4	(-0.0076± 0.1317 j) ×10^4
3,4	(-0.0089 ± 0.1295 j) ×10^4	(-0.0214 ± 0.1333 j) ×10^4
5,6	(-0.0124± 0.1401 j) ×10^4	(-0.0898 ± 1.9927 j) ×10^4
7,8	(-0.0915 ± 1.8589 j) ×10^4	(-0.0770 ± 3.5620 j) ×10^4
9,10	(-0.0729 ± 3.1183 j) ×10^4	**(2.4248 ± 7.3828 j) ×10^4**
11,12	(-0.0747 ± 6.6933 j) ×10^4	**2.5886×10^4**, -5.5608×10^4

TABLE II
POLES ZEROS PATTERN OF PZT NOMINAL MODEL

	Poles	Zeros
1,2	(-0.0488 ± 3.1141j) ×10^4	(-0.0056 + 0.3132j) ×10^5
3,4	(-0.0869 ± 4.1066j) ×10^4	(-0.0168 + 0.4239j) ×10^5
5,6	(-0.2287 ± 5.1408j) ×10^4	(-0.0267 + 0.5234j) ×10^5
7,8	(-0.0320 ± 6.7123j) ×10^4	(-0.0588 + 0.7707j) ×10^5
9,10	(-1.4642 ± 8.4616j) ×10^4	**1.2430×10^5**, -4.3606×10^5

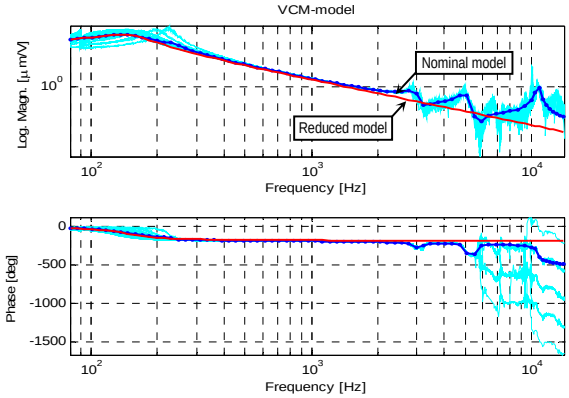

Fig. 2. The frequency response estimates for the VCM, the nominal model and its reduced form.

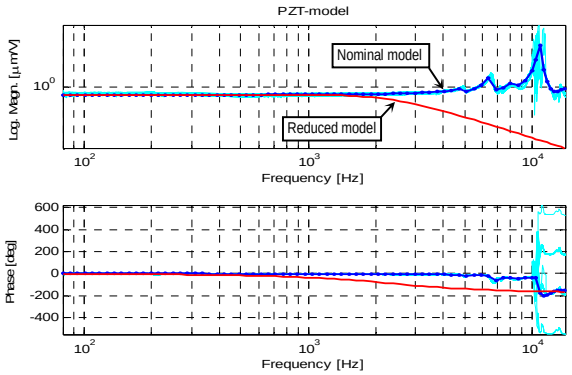

Fig. 3. The frequency response estimates for the PZT, the nominal model and its reduced form.

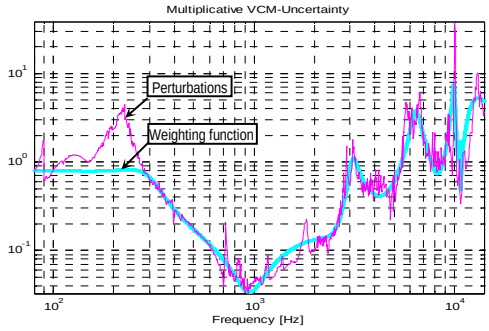

Fig. 4. The multiplicative uncertainty profile of the VCM

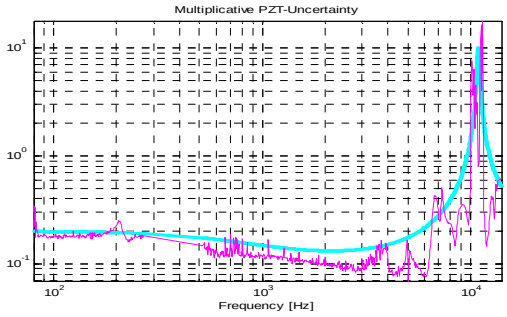

Fig. 5. The multiplicative uncertainty profile of the PZT

derived and using equation (2) the uncertainty profiles are calculated for each actuator and illustrated in figures 4 and 5, respectively. As it will be elaborated in the proceeding section, the adaptive robust controller for the system is designed based on a reduced order model of the system. Hence the full order model of the system and its uncertainty profile is used in simulation to verify the robustness of the proposed algorithm in presence of modelling uncertainty.

III. Adaptive Robust Control

In order to design the adaptive robust controller, identification of a simple model for the system is sufficient [10]. The comprehensive models for actuators can be reduced to second-order transfer functions as illustrated in figures 4 and 5. The state space representation of such models can be linearly parameterized as:

$$\dot{x}_1 = x_2 \tag{3}$$

$$\theta_1 \dot{x}_2 = u - \theta_2 x_2 - \theta_3 Sign(x_2) + \theta_4 + \tilde{d} \tag{4}$$

In which $\theta_4 = d_n$ is the nominal value of the lumped disturbance d. It is assumed that, all the effect of unmodeled dynamics, hysteresis and high frequency resonances of the systems are absorbed into the term d. In order to describe the controller structure, consider the following assumptions.

Assumptions: The following bounds and structures for uncertainties and disturbances are assumed.

$$\theta \in \Omega_\theta \equiv \{\theta : \theta_{\min} < \theta < \theta_{\max}\}$$
$$\tilde{d} \in \Omega_d \equiv \{\tilde{d} : |\tilde{d}| < \delta_d\} \tag{5}$$

In which, $\theta_{\min} = [\theta_{1\min}, ..., \theta_{4\min}]^T$, $\theta_{\max} = [\theta_{1\max}, ..., \theta_{4\max}]^T$ and δ_d are assumed to be known. Let $\hat{\theta}$ denotes the estimate of θ and $\tilde{\theta}$ the estimation error (i.e. $\tilde{\theta} = \hat{\theta} - \theta$). In view of (4) the following adaptation law with discontinuous projection modification can be used:

$$\dot{\hat{\theta}} = \Pr oj(\Gamma \tau) \tag{6}$$

where, $\Gamma > 0$ is a diagonal matrix, τ is adaptation function to be synthesized later. The projection mapping is defined as:

$$\Pr oj_{\hat{\theta}}(\bullet) = [\Pr oj_{\hat{\theta}_1}(\bullet_1), ..., \Pr oj_{\hat{\theta}_p}(\bullet_p)]^T$$
$$\Pr oj_{\hat{\theta}_i}(\bullet_i) = \begin{cases} 0, (if\ \hat{\theta}_i = \theta_{i\max}\ \&\ \bullet_i > 0) or (if\ \hat{\theta}_i = \theta_{i\min}\ \&\ \bullet_i < 0) \\ \bullet_i \qquad Otherwise \end{cases} \tag{7}$$

It can be shown that for any adaptation function τ the projection mapping used in (7) guarantees [10]:

$$P1 \quad \hat{\theta} \in \Omega_\theta \equiv \{\hat{\theta} : \theta_{\min} \le \hat{\theta} \le \theta_{\max}\}$$
$$P2 \quad \tilde{\theta}^T(\Gamma^{-1} \Pr oj(\Gamma\tau) - \tau) \le 0 \quad \forall \tau \tag{8}$$

A. ARC Controller Design

Define a PD switching-function as $p = \dot{e} + k_1 e = x_2 - x_{2eq}$, where $x_{2eq} \equiv \dot{y}_d - k_1 e$ and $e = y - y_d(t)$ is the output tracking error, $y_d(t)$ is the desired trajectory to be tracked by y, and k_1 is any positive feedback gain. With respect to (3) one can obtain:

$$J\dot{p} = u - \theta_1 \dot{x}_{2eq} - \theta_2 x_2 - \theta_3 Sign(x_2) + \theta_4 + \tilde{d} = u + \varphi^T \theta + \tilde{d} \tag{9}$$

If p is small or converges to zero exponentially, then the output tracking error e, will be small or converges to zero

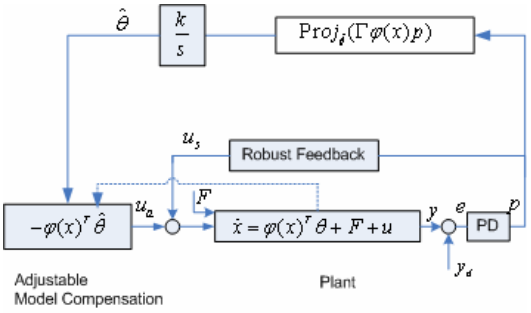

Fig. 6. ARC Block diagram

exponentially. This is because $G_p(s) = e(s)/p(s) = 1/(s+k_1)$ is a stable transfer function. Hence, the rest of design is to make p as small as possible. Where $\varphi^T = [-\dot{x}_{2eq}, -x_2, -Sign(x_2), 1]$ and $\dot{x}_{2eq} = \ddot{y}_d - k_1\dot{e}$.

The control law consists of two parts:

$$u = u_a + u_s \qquad u_a = -\varphi^T\hat{\theta}$$
$$u_s = u_{s1} + u_{s2} \qquad u_{s1} = -k_2 p \tag{10}$$

Where u_a is the adjustable model compensation needed for achieving perfect tracking, and u_s is a robust control law consist of two parts: u_{s1} is used to stabilize the nominal system which is a proportional feedback in this case, and u_{s2} is a robust feedback term to attenuate the effect of model uncertainties, which will be synthesize later. Substituting (10) in to (9), and simplifying one can obtain:

$$J\dot{p} = u_s - \varphi^T\tilde{\theta} + \tilde{d} \tag{11}$$

Noting Assumption 1 and P1 of (8), there exist a u_{s2} such that the following two conditions are satisfied:

$$i)\, p\{u_{s2} - \varphi^T\tilde{\theta} + \tilde{d}\} \le \varepsilon \qquad ii)\, pu_{s2} \le 0 \tag{12}$$

where, ε is a design parameter which can be chosen arbitrarily small. From condition (i) u_{s2} is synthesized to dominate the model uncertainties coming from both parametric uncertainties $\tilde{\theta}$ and uncertain nonlinearities $\tilde{d}$, and condition (ii) guarantees that u_{s2} is dissipative in nature so that it does not interfere with the functionality of the adaptive control part u_a. If the adaptation function in (6) is chosen as $\tau = \varphi.p$ then the ARC control law in (10), whose general block diagram is depicted in Fig. 6, guarantees all signals to be bounded [10]. In addition, if after finite time t_0, there exist only parametric uncertainties i.e., ($\tilde{d} = 0, \forall t \ge t_0$), then zero final tracking error is achieved, i.e. $e \to 0$ and $p \to 0$ as $t \to \infty$.

B. Improved Desired Compensation ARC

In the ARC design presented, the regressor φ in the model compensation u_a (Eq. 10) and adaptation function $\tau = \varphi.p$ depends on the actual measurement of the velocity x_2. Thus the effect of measurement noise is severe. Moreover, in spite of condition ii of (12), there still exist certain interaction between the model compensation u_a and the robust control

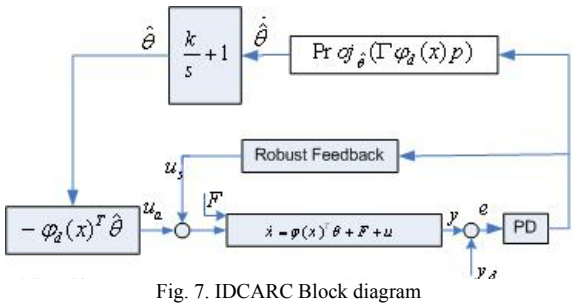

Fig. 7. IDCARC Block diagram

u_s. This may complicate controller gain tuning process in an experimental implementation. In the IDCARC, the control law and the adaptation function have the same form as (10) and $\tau = \varphi.p$, respectively, however, regressor φ is substituted by the desired regressor φ_d:

$$u = u_a + u_s \qquad u_a = -\varphi_d^T\hat{\theta} \qquad \tau = \varphi_d p \tag{13}$$

Where $\varphi_d^T = [-\ddot{y}_d, -\dot{y}_d, -Sign(\dot{y}_d), 1]$. Substituting (13) into (11) and noting that $x_2 = \dot{y}_d + \dot{e}$, one obtains:

$$J\dot{p} = u_s - \varphi_d^T\tilde{\theta} + \underline{(\theta_1 k_1 - \theta_2)\dot{e} + \theta_3[Sign(\dot{y}_d) - Sign(x_2)]} + \tilde{d} \tag{14}$$

Note that since only the desired trajectory information $y_d(t)$ is needed in this case, the effect of noise is reduced significantly. Comparing (14) with (11), it can be seen that two additional terms (under lined) has been appeared, which may demand a strengthened robust control function u_s for a robust performance. The strengthened robust control function u_s has the same form as (10):

$$u_s = u_{s_1} + u_{s_2} \qquad u_{s_1} = -k_{s_1} p \tag{15}$$

The drawback of using desired regressor φ_d instead of measured one φ, is the inability to attenuate disturbance fast enough to accommodate hard disk drives requirements. This is remedied in IDCARC by using a dynamical adaptation law. As depicted in Fig. 8 it is proposed to change the *I* (integrator) estimator with a *PI* (Proportional-Integral) routine in estimation mechanism of θ. A detail elaboration of the effect of these changes into the identification procedure, and a thorough stability analysis of this algorithm is given in [10].

C. Reduced Order Model and Prefilter Design

As it is described in the previous subsections, in order to design ARC controllers for each actuator of the HDD, a reduced second-order model for each actuator is needed. As it is illustrated in figures 3, and 4, the reduced order models are assigned as the following transfer functions.

$$G_{VCM,reduced} = \frac{8.119\times10^7}{s^2 + 460.3s + 853776}\,\mu m/Volt \tag{16}$$

$$G_{PZT,reduced} = \frac{1.343\times10^8}{s^2 + 21000s + 2.25\times10^8}\,\mu m/Volt \tag{17}$$

One of main features neglected in these reduced models is the effect of non-min phase zeros of the models, which are given in Tables I and II. The destabilising effect of neglecting those zeros can be compensated by designing appropriate prefilters in addition to the usual ARC structure of the controllers for

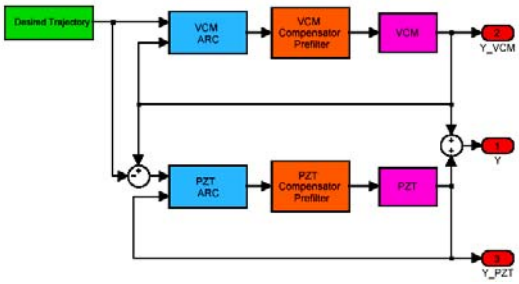

Fig. 8. The VCM and PZT final controller strategy.

each actuator as depicted in Fig. 8. The prefilters are designed by carefully examination of the location of the unstable zeros of the models, and also the uncertainty profile of the system (Figures 4 and 5). As a direct implication of small-gain theorem for the robust stability of uncertain systems, it is well understood that at the frequencies where the uncertainty profile of the system is beyond zero dB, the designed controller must reduces $||WT||_\infty<1$, in which $W(s)$ is the uncertainty weighting function and $T(s)$ is the closed loop transfer function.

To accomplish that for the VCM prefilter design, consider the following fourth order stable transfer function with relative degree two, whose poles are located close to the high frequency stable and the mirror of unstable zeros of the plant with respect to the imaginary axis, and its zeros are close to the high frequency poles of the system:

$$P_{VCM} = K_1 \frac{s+(0.07\pm 6.7j)\times 10^4}{(s+5.56\times 10^4)(s+2.6\times 10^4)(s+(2.4\pm 7.4)\times 10^4)} \qquad (29)$$

K_1 is chosen such that the DC gain of the transfer function equals to one. Similarly for the PZT actuator a sixth order stable transfer function with relative degree of two is designed. The prefilter zeros compensate for the high frequency poles of the system, and its poles compensate for high frequency stable and unstable zeros of the system. Moreover, a pair of complex poles with $\omega=1.5e4$ *rad/sec,* $\xi=0.707$ is added to the prefilter to act as the dominant poles for the system in controller design. K_2 is chosen such that the DC gain of the transfer function equals to one.

$$P_{PZT} = K_2 \frac{(s+(0.03\pm 6.7j)\times 10^4)(s+(1.4\pm 8.4j)\times 10^4)}{(s^2+2\omega\xi s+\omega^2)(s+(0.58\pm 7.7)\times 10^4)(s+1.24\times 10^5)(s+4.36\times 10^5)} \qquad (30)$$

The bode plots of VCM, and PZT actuators, with and without prefilter compensation is given in figures 9, and 10, respectively. As it is shown in this figure, the prefilters attenuates the system gains at high frequencies, where the uncertainty profiles are higher than 0 dB, while adding negative phase to the systems to compensate for destabilizing effect of unstable zeros of the systems.

IV. Simulation Results

A. Performance Indices

Simulations studies have been performed for ARC, and IDCARC to verify the effectiveness of the proposed controller in terms of tracking errors, and disturbance rejection in

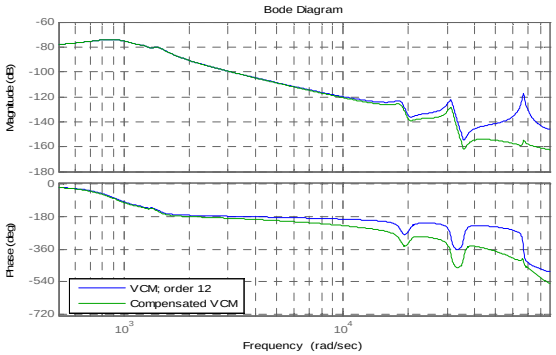

Fig. 9. The bode plot of the VCM 12th order model with and without prefilter compensation

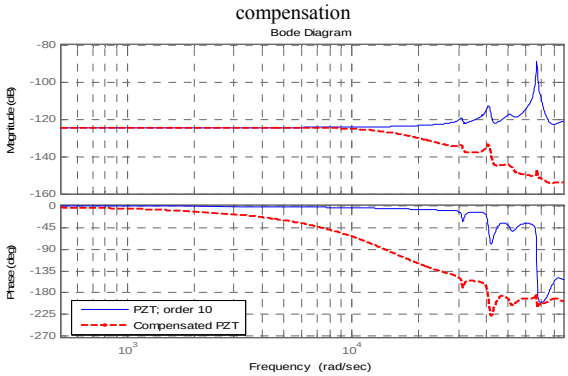

Fig 10. The bode plot of the PZT 10th order model with and without prefilter compensation

presence of modelling uncertainty. In order to compare simulation results the following performance indices are used.

I1) $L_2[e]=\left[1/T_f\cdot\int_0^{T_f}|e|^2\,dt\right]^{1/2}$ is an average tracking performance index, for the entire error curve $e(t)$, and T_f represents the total simulation time.

I2) $e_M=\max_t\{|e(t)|\}$, is the maximum absolute value of the tracking error, and is a measure of transient performance.

I3) $e_F=\max_{T_{f-1}\le t\le T_f}\{|e(t)|\}$, is the maximum absolute value of the tracking error during the last one millisecond.

I4) $L_2[u]=\sqrt{1/T_f\int_0^{T_f}|u|^2\,dt}$, is the mean of the control input.

I5) $c_u=L_2[\Delta u]/L_2[u]$, is the control input chattering, where $L_2[\Delta u]=\sqrt{1/N\sum_{j=1}^{N}|u(j\Delta T)-u((j-1)\Delta T)|^2}$ is the normalized control variations.

B. Controller Structures

The following control structures are used in simulations:

• **ARC:** The ARC law proposed in section 3. is applied on both actuators. With $u_s=-k_sp$, $k_s\ge k_2+h^2/4\varepsilon$ *and* $k_s=1.0$, the PD switching control gains are chosen as given below in order to obtain closed loop bandwidth of 1kHz, and 70kHz for VCM, and PZT actuator, respectively

$C_{PD,VCM}=48.52s+4.909\times 10^4$, $C_{PD,PZT}=74.76s+1.135\times 10^5$

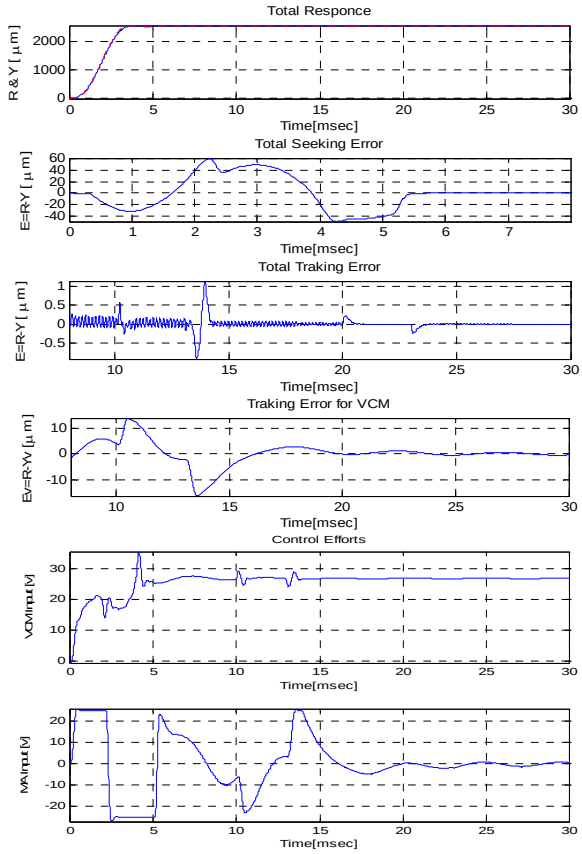

Fig. 11. The closed loop performance of the ARC controller in presence of disturbance

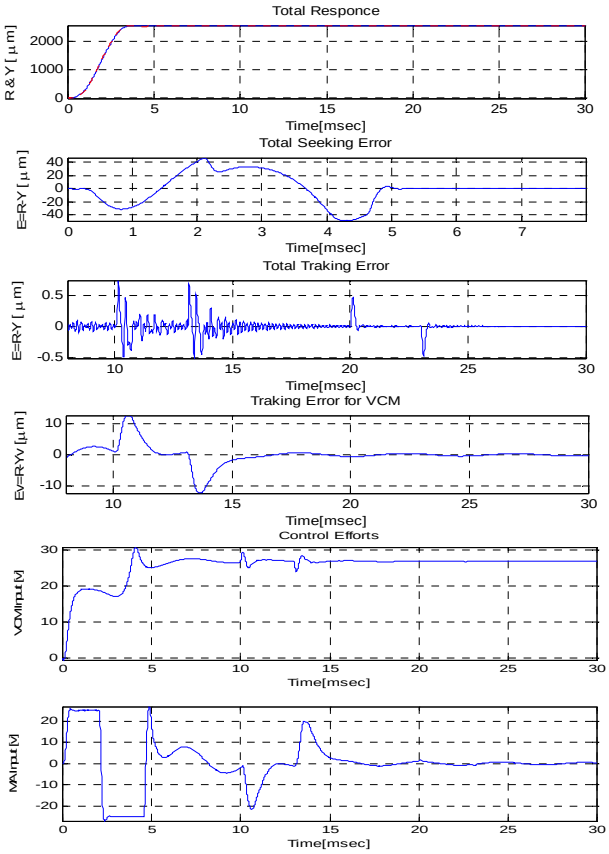

Fig. 12. The closed loop performance of the IDCARC controller in presence of disturbance

The adaptation rates are set as Γ=diag[10 100 1e5 100], and the initial parameters are chosen as follows:

$\theta_{VCM} = \begin{bmatrix} 0.01231 & 5.6695 & 1.0515\times10^{4} & 1 \end{bmatrix}$

$\theta_{PZT} = \begin{bmatrix} 7.4458\times10^{-3} & 1.5636\times10^{2} & 1.6753\times10^{6} & 1 \end{bmatrix}$

• **IDCARC:** The proposed IDCARC law is applied on the system. All coefficients are the same as ARC coefficient and the integrator gain in the adaptive part is set to k_I=*1000*.

C. Simulation Input Signals

In order to verify the effectiveness of the proposed controller in obtaining the stringent tracking performance requirement the following two sets of experiments considered for the system.

Set 1*:* To test tracking performance of the controllers in presence of disturbances acting on the system, a 2600 track seeking trajectory is considered in this set. The reference trajectory is designed based on SMART algorithm described in [10], and is illustrated in Fig. 11. Moreover, the following pulse disturbance inputs for VCM and PZT are applied, at 0.01 sec, and 0.02 sec, respectively.

$d_{vcm} = 3\big(u(t-0.01)-u(t-0.013)\big)$, $d_{pzt} = 2\big(u(t-0.020)-u(t-0.023)\big)$

The saturation amplitude of the PZT actuator is considered as ±*25 volts*.

Set 2*:* The performance of the closed loop system to the Set 1 reference trajectory, is simulated in this set in the presence of worst case uncertainty at both actuator models $\|\Delta\|_\infty$=1. This set is considered to verify the robust performance of the proposed controller.

D. Controllers Performance

Figures 11 and 12 illustrate the closed loop performance of the ARC and the proposed controller, respectively. In these simulations the disturbance rejection objective, which is designed in Set 1, is simulated for the full order nominal model of VCM and PZT servo actuators. In order to have detail comparison of the controller performances different quantities are plotted in these figures. The total tracking performance of the tip head for 2600 one micron tracks are plotted first versus the desired trajectory.

The tracking errors are divided into two next plots in these figures, in which in the first plot the total seeking performance for the first 8 millisecond seeking time is given, while the accuracy of the tip positioning in tracking performance is given in the next plot. To evaluate the significance of the PZT actuator in order to reduce the tracking performance of the total head tip position, the VCM tracking performance is given separately in the next plot, and finally, the actuator efforts of the VCM and PZT actuators are given in the last two plots. To further compare the controller performances

TABLE III
PERFORMANCE INDEX FOR DESIRED TRAJECTORY

Experiments	Set 1				Set 2			
Performance	ARC		IDCARC		ARC		IDCARC	
Index	VCM	PZT	VCM	PZT	VCM	PZT	VCM	PZT
$e_M \times 10^{-5}$	6.4	6.1	4.8	4.7	9.6	8.4	7.5	6.3
$\mathbf{e_F \times 10^{-7}}$	**4.5**	**0.06**	**3.1**	**0.04**	**127.5**	**127.5**	**6.9**	**0.01**
$L_2[e]\times 10^{-4}$	9.2	8.0	7.2	6.1	28.3	24.8	17.3	15.4
$L_2[u]\times 10^{2}$	14.2	7.0	14.2	6.0	73.7	13.6	130.2	16.6
$L_2[\Delta u]\times 10^{-2}$	9.8	0.31	6.5	0.32	0.10	8.97	6.18	8.4
$c_u \times 10^{-4}$	69.1	4.5	0.46	5.4	0.13	0.66	0.047	0.51

quantitatively, the performance indices described in the preceding section is given in Table III. The final error performance index is highlighted in this table, which indicates the final tracking error achievable by the controller, and the individual contribution of VCM and PZT actuator to this performance.

It is observed that the proposed method is contributing into a better tracking performance in both seeking and tracking regimes, and the effect of disturbance is rejected significantly reaching to a final tracking error *4e-3* microns in the IDCARC method. However, the difference between the closed-loop performance of ARC and IDCARC are minimal in these simulations. The significant improvement of introducing dynamic adaptation in the proposed method is revealed in the simulation of Set 2, in which the worst case modelling uncertainty is also integrated into simulations. Figures 13 and 14 compares the closed loop performance of ARC and IDCARC methods in presence of modelling uncertainty, and the quantitative evaluation of the performance indices are given in Table III. As it is seen in these figures, the ARC controller is unable to reduce the final tracking performance below one micron, and as it is seen in the actuator effort of PZT remains in saturation for all the simulation time. However, the IDCARC controller preserves the total tracking error below one micron, and as it is specified in Table III, the final tracking error for this case is increased to *1e-2* microns, which is completely satisfying, while the control efforts of both actuators remain also within their limits. These extraordinary results are reproduced for disturbance rejection objective with worst case uncertainty, and are very promising for physical implementation.

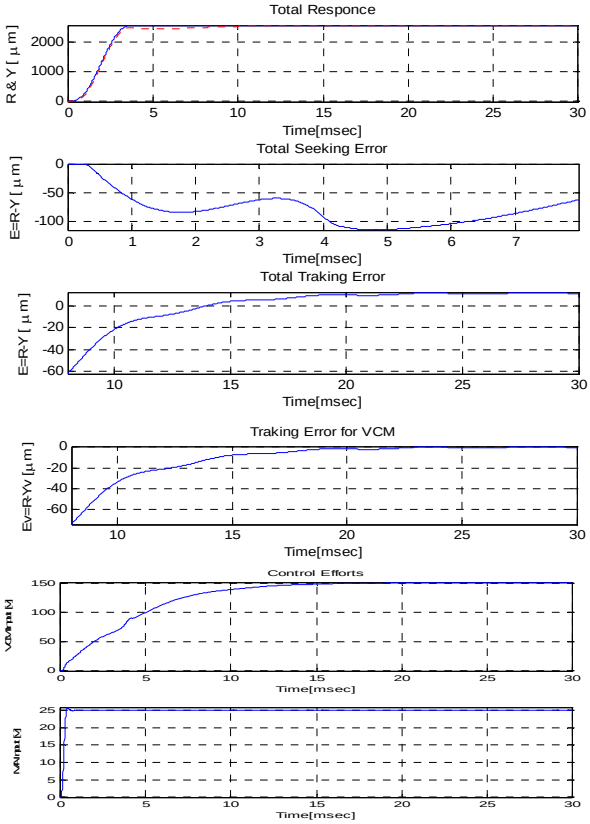

Fig. 13. The closed loop performance of the ARC controller in presence of worst case uncertainty

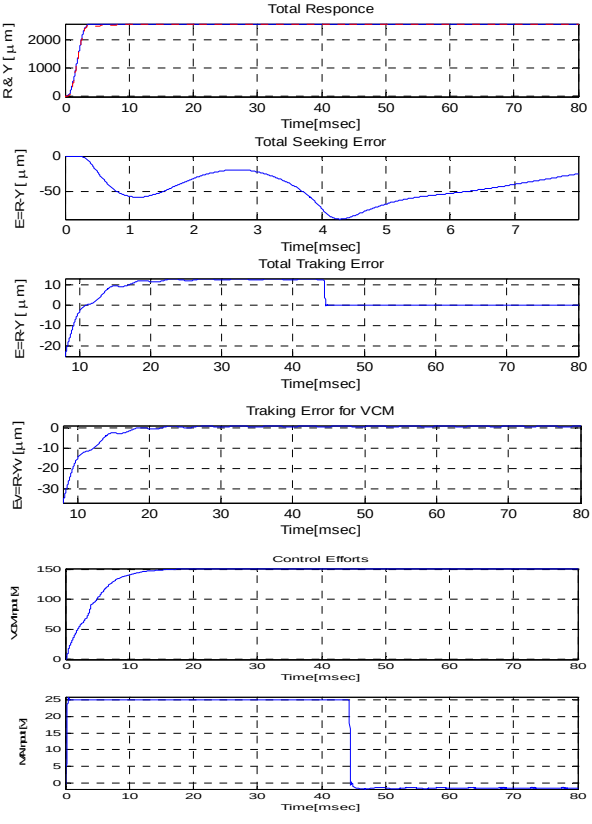

Fig. 14. The closed loop performance of the IDCARC controller in presence of worst case uncertainty

V. CONCLUSIONS

In this paper, an adaptive robust controller is implemented on dual-stage hard disk drives. An adaptive robust controller (ARC) is designed first for each actuator, which theoretically guarantees a prescribed transient performance and well behaved tracking in presence of uncertainties. An IDCARC scheme is then proposed, in which a dynamic adaptation law is included into the ARC method. A robust simulation study of these method are presented in this paper, in which the controllers designed based on simple models for the subsystem are implemented on an experimentally verified high order models for the system. Simulation result verifies the effectiveness of the IDCARC method in preserving the stringent tracking performance requirement of the hard disk drives in presence of worst case unstructured uncertainty of the models. This analysis provides the required assurance of its successful experimental implementation in future.

ACKNOWLEDGMENT

We are thankful and in debt to the authors of the reference paper [11] who provide us with the detail experimental data of VCM and PZT actuators.

REFERENCES

[1] Numasato, H. and Tomizuka, M., Settling control and performance of a dual-actuator system for hard disk drives, IEEE/ASME Transactions on Mechatronics, v 8, n 4, Dec. 2003, p 431-8.

[2] K. Mori, T. Munemoto, H. Otsuki, Y. Yamaguchi, and K. akagi, A dual-stage magnetic disk drive actuator using a piezoelectric device for high track density, IEEE Trans. Magn, vol 27, pp 5298-5300, Dec. 1991.

[3] Yaolong Lou, Peng Gao; Bin Qin; Guoxiao Guo; Eng-Hong Ong; Takada, A.; Okada, K. Dual-stage servo with on-slider PZT microactuator for hard disk drives, IEEE Transactions on Magnetics, v 38, n 5, pt.1, Sept. 2002, p 2183-5.

[4] D. Hernandez, S. Park, R. Horowitz, and K. Packard, Dual-stage track following servo design for hard disk drives, American Control Conference, pp 4116-21, 1991.

[5] X. Hu, W. Guo, T. Huang, and B.M. Chen, Discrete-time LQG/LTR dual-stage controller design and implementation for high track density HDDs, American Control Conference, pp 4111-15, 1991.

[6] Ben M. Chen, Tong H. Lee, V. Venkataramanan, Composite nonlinear feedback control for linear systems with input saturation theory and application, IEEE Trans. Automatic Control, 48(3), 2003, 427-439.

[7] Q. Hao, R. Chen, G. Guo; S. Chen; T. S. Low, A gradient-based track-following controller optimization for hard disk drive, IEEE Transactions on Industrial Electronics, 50(1), 2003, 108 – 115.

[8] C. Du, L. Xie, J.N. Teoh, G. Guo, An Improved Mixed H2/H∞ Control Design for Hard Disk Drives, IEEE Transactions on Control Systems Technology, 13(5) 2005, 832 – 839.

[9] B. Yao, M. Tomizuka, Smooth robust adaptive sliding mode control of robot manipulators with guaranteed transient performance, Trans. ASME, J. Dyn. Syst., Meas. Cont., 118(4), 1996, 764-775.

[10] E. Jamei, H.D. Taghirad, Adaptive robust controller synthesis for hard disk servo systems, In Proc. IEEE/RJS, Conf. on Intelligent Robots and Systems, Sendai, Japan, 2004, 1154-1159.

[11] Herrmann, G.; Turner, M.C.; Postlethwaite, I.; Guoxiao Guo, Practical implementation of a novel anti-windup scheme in a HDD-dual-stage servo-system, IEEE/ASME Transactions on Mechatronics, Volume 9, Issue 3, Sept. 2004 Page(s):580 – 592

[12] H.D. Taghirad and P.R. Belanger, "H∞-Based robust torque control of harmonic drive systems", Journal of Dynamic Systems, Measurements and Control, 123(3): 338-345, 2001.